RSC Advances

PAPER

View Article Online
View Journal | View Issue

Cite this: *RSC Adv.*, 2025, **15**, 38218

# Developing the half-metallic ferromagnetism in semimetal germanene monolayer: synergistic effects of band gap opening and magnetism engineering

Duy Khanh Nguyen, [ab] R. Ponce-Pérez,[c] J. Guerrero-Sanchez[c] and D. M. Hoat [*de]

Similar to graphene, the germanene monolayer could be a promising two-dimensional (2D) platform for spintronic applications. In this work, efficient doping routes are proposed to develop the half-metallic ferromagnetism in the germanene monolayer, based on the synergistic effects of band gap opening and magnetism engineering. The pristine germanene monolayer is a semimetal, exhibiting a Dirac cone originating mainly from the Ge-$p_z$ state. The band gap opening can be achieved by doping with chalcogen atoms. Specifically, single S and Se impurities give a direct gap of 0.28 and 0.27 eV, respectively. This parameter increases up to 0.50 and 0.49 eV, respectively, when increasing the doping level. Moreover, Mn doping induces significant magnetism in the germanene monolayer with an overall magnetic moment of $3.78\mu_B$ produced primarily by the Mn impurity. Herein, the antiferromagnetic semiconductor nature is obtained with a small energy gap of 0.05 eV. Further incorporating additional S and Se impurities causes a transition from the antiferromagnetic semiconductor state to a ferromagnetic half-metallic state, suggesting successful development of half-metallic ferromagnetism in the germanene monolayer. In these cases, the spin-down energy gap has values of 0.24 and 0.26 eV, respectively, while the spin-up state exhibits metallic character. Along with the state transition, codoping with chalcogen impurities also induces the switching from perpendicular magnetic anisotropy to in-plane magnetic anisotropy, which is of great importance for magnetic field sensing. In addition, our simulations confirm good thermodynamic stability of all the doped germanene systems. Our findings may introduce promising 2D spintronic materials with the desired half-metallic ferromagnetism, which can be prepared by codoping the germanene monolayer with chalcogen atoms and Mn transition metal.

Received 15th August 2025
Accepted 18th September 2025

DOI: 10.1039/d5ra06032j

rsc.li/rsc-advances

## 1. Introduction

In early studies, the prediction of graphene was carried out by Wallace *et al.*[1] using tight-binding calculations. The authors demonstrated the semimetal nature of graphene formed by the coincidence of the valence band maximum point and conduction band minimum point at the Fermi level. However, it was not until 2004 that the first exfoliation of graphene was successfully carried out by Novoselov *et al.*,[2] and this two-dimensional material has since attracted increasingly great attention. Graphene consists of carbon atoms arranged in a honeycomb-like planar structure, in which $sp^2$ hybridization and quantum confinement originate unprecedented intriguing physical, chemical, and mechanical properties.[3,4] Located in the same IVA-group of the periodic table with similar valence electronic configuration, it can be expected that the 2D form of germanium – germanene – could also exhibit $sp^2$ hybridization with the same structure as graphene. However, Takeda *et al.*[5] have predicted the hexagonal structure of germanene but it is not planar, but corrugated. This structural corrugation suggests that the electronic interactions are mixed $sp^2/sp^3$ rather than only $sp^2$. Then, tight-binding based theoretical calculations have demonstrated the semimetal nature of germanene with a Dirac cone at the K point.[6] Theoretical results have motivated great efforts to synthesize germanene. Since there is no layered structure of germanium in nature, germanene has been prepared mostly by bottom-up methods. The first experimental success in synthesizing germanene was reported in 2014 by Li

---

[a] *Laboratory for Computational Physics, Institute for Computational Science and Artificial Intelligence, Van Lang University, Ho Chi Minh City, Vietnam. E-mail: khanh.nguyenduy@vlu.edu.vn*

[b] *Faculty of Mechanical, Electrical and Computer Engineering, Van Lang School of Technology, Van Lang University, Ho Chi Minh City, Vietnam*

[c] *Universidad Nacional Autónoma de México, Centro de Nanociencias y Nanotecnología, Apartado Postal 14, Ensenada, Baja California, 22800, Mexico*

[d] *Institute of Theoretical and Applied Research, Duy Tan University, Ha Noi 100000, Vietnam. E-mail: dominhhoat@duytan.edu.vn*

[e] *School of Engineering and Technology, Duy Tan University, Da Nang 550000, Vietnam*

*et al.*[7] Then, quasi-freestanding germanene has been successfully prepared in experiments.[8,9] So far, many research groups have succeeded in fabricating germanene,[10–13] exploring this 2D germanium counterpart as a promising candidate for diverse applications.[14,15]

Similar to graphene, the absence of an intrinsic band gap in germanene may hinder its practical applications. Therefore, band gap opening may be considered as an important functionalization step at the time of designing its applications. Ni *et al.*[16] have predicted a vertical electric field as an able route to open the germanene band gap using *ab initio* calculations. It was found that the band gap size increases linearly with the electric field strength. Besides, chemical modification has been also widely proposed. For example, the adsorption of alkali metals can induce a tunable band gap ranging from 0.02 to 0.31 eV in germanene.[17] Large band gaps between 0.416 and 1.596 eV can be obtained in the germanene monolayer by full- or Janus-halogenation.[18] Hydrogenation is also an effective method to open the germanene band gap that has been confirmed both theoretically and experimentally.[19,20]

On the other hand, silicon-based traditional electronic devices have been considerably replaced by spintronic devices that use electron spin as the main information carrier, and these spintronic devices have emerged as a promising solution to the demands of the rapid advancements in information storage and processing.[21,22] In the spintronics field, 2D materials are ideal platforms for the design of new low-dimensional spintronic materials with intriguing magnetism and novel physical effects.[23–25] In this regard, some transition-metal-containing 2D magnetic materials with intrinsic magnetism have been exploited.[26–28] However, a large number of the experimentally fabricated and theoretically predicted 2D materials are intrinsically nonmagnetic, therefore magnetism engineering has been also extensively investigated in order to make new 2D spintronic materials. In particular, it has been found that doping with transition metals induces significant magnetic properties in the germanene monolayer;[29] however developing half-metallic ferromagnetism in the semimetal germanene monolayer with perfect spin polarization at the Fermi level – a highly desirable feature for spintronic applications – still is a challenge.

In this work, we predict the half-metallic ferromagnetism in the germanene monolayer using first-principles calculations. This interesting physical property is obtained when combining the band gap opening induced by chalcogen (S and Se) doping and magnetism engineering achieved by Mn doping. In addition, in-plane magnetic anisotropy also suggests the proposed codoping as an effective route to functionalize the germanene monolayer towards applications in magnetic field sensing.

## 2. Computational details

All calculations are performed within the framework of spin-polarized density functional theory (DFT),[30] and are based on the projector augmented wave method as embedded in the Vienna *ab initio* simulation package.[31,32] Within the generalized gradient approximation, electron exchange–correlation effects are treated with the Perdew–Burke–Ernzerhof (PBE) formula (GGA-PBE).[33] In consideration of the strong correlation of Mn-3d electrons, the DFT+$U$ method[34] is adopted using an effective Hubbard parameter of 3.90 eV that is based on previous theoretical calculations.[35,36] Our testing shows good convergence of the total magnetic moment using this value (see Fig. S1 of the SI). Energy cutoff of 500 eV is set for the plane wave expansion. Total system energy is set to converge to $10^{-6}$ eV for self-consistent iterations. The structural relaxation is carried out until residual forces acting on each atom fall below $10^{-2}$ eV Å$^{-1}$. A 4 × 4 × 1 supercell is generated to simulate the doping cases in the germanene monolayer. Monkhorst–Pack $k$-point grids[37] of 20 × 20 × 1 and 4 × 4 × 1 are chosen for the germanene unit cell and 4 × 4 × 1 supercell, respectively. The employed cutoff energy and $k$-point mesh have been tested to provide good convergence of the ferromagnetic half-metallic codoped systems (see Fig. S2 of the SI). Gaussian smearing with a width of 0.05 eV is employed (ISMEAR = 0 and SIGMA = 0.05), except for the calculations of density of states that are carried out using the tetrahedron method with Blöchl corrections without smearing (ISMEAR = −5). A vacuum space more than 20 Å perpendicular to the germanene monolayer plane is inserted to separate two adjacent monolayer images in order to avoid spurious interactions between them.

## 3. Results and discussion

### 3.1. Structural and electronic properties of the germanene monolayer

Fig. 1 shows the atomic structure of the germanene monolayer in a 4 × 4 × 1 supercell. It can be noted that the Ge atoms are arranged in a honeycomb lattice similar to graphene (top-view), presenting the structural buckling height as a clear difference (side-view). After realizing the structural relaxation for the germanene monolayer unit cell, the following parameters are obtained: (1) lattice constant $a = 4.01$ Å; (2) chemical bond length $d_{\text{Ge–Ge}} = 2.42$ Å; (3) buckling height $\Delta_{\text{Ge–Ge}} = 0.71$ Å; and (4) interatomic angle $\angle\text{GeGeGe} = 111.87°$, which are in good agreement with previous theoretical studies.[38]

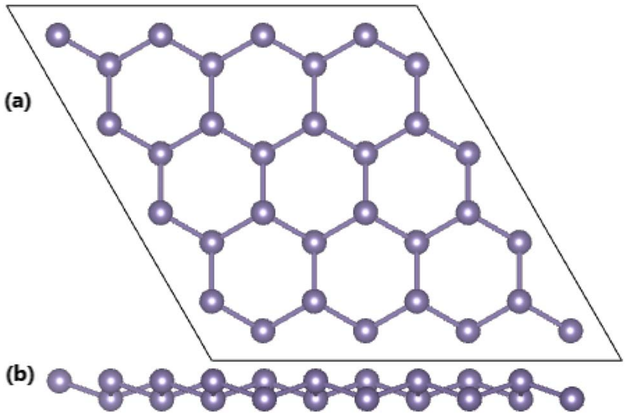

Fig. 1 (a) Top-view and (b) side-view of the atomic structure of the germanene monolayer in a 4 × 4 × 1 supercell.

The orbital-decomposed band structure of the germanene monolayer is displayed in Fig. 2a. The semimetal nature formed by the coincidence of the valence band maximum energy level and conduction band minimum energy level at the K point can be noted. This electronic feature is produced mainly by the Ge-$p_z$ state that originates the electronic subband around the K point, while the Ge-$p_x$ and Ge-$p_y$ states form mainly the valence subband around the Γ point. Moreover, the Ge-s state makes a contribution mainly in the conduction band. In addition, the electron localization function visualized in Fig. 2b demonstrates the covalent character of the Ge–Ge chemical bond, considering the considerable electron accumulation between the Ge atoms that is a characteristic of monoelemental monolayers.[39]

### 3.2. Effects of doping with chalcogen atoms

In this part, the impact of chalcogen (X = S or Se) doping on the germanene monolayer's electronic properties is studied. Firstly, single atom doping is considered, where the doped systems are denoted as 1X@mo. The electronic interactions between the chalcogen impurities and the germanene monolayer are analyzed by calculating the charge density difference $\Delta\rho$ as follows: $\Delta\rho = \rho(1X@mo) - \rho(mo) - \rho(X)$, where $\rho(1X@mo)$, $\rho(mo)$, and $\rho(X)$ are the charge density of the 1X@mo system, germanene monolayer, and single X atom, respectively. Results are visualized in Fig. 3. Note that the Ge atoms closest to the doping sites lose charge, while charge enrichment is observed at chalcogen sites and the region between the X and Ge atoms. The charge accumulations at X impurities can be attributed to the charge transfer from Ge atoms to X atoms because of the electronegativity difference (X atoms are more electronegative than the Ge atom), generating the ionic character of the X–Ge bond. Quantitatively, Bader charge analysis indicates that S and Se impurities attract charge quantities of 0.73 and 0.54*e* from the host germanene monolayer, respectively. In addition, considerable charge accumulation in the interatomic regions also gives a signal of the covalent character of the X–Ge bond.

Our spin-polarized calculations provide that chalcogen doping induces no magnetism in the germanene monolayer, where the 1X@mo doped systems have zero total and local magnetic moments. The preservation of the nonmagnetic nature of the germanene monolayer is also reflected in the equally spin-distributed charge, such that the band structures and projected density of states (PDOS) spectra are spin-symmetric as seen in Fig. 4. Importantly, chalcogen doping opens the germanene monolayer band gap, where the valence band maximum and conduction band minimum at the K point suggest the direct-gap semiconductor nature of the 1X@mo systems. Specifically, single S and Se impurities induce band gaps of 0.28 and 0.27 eV, respectively. PDOS spectra indicate significant hybridization between S(Se)-p and Ge-p orbitals in the upper part of the valence band and the lower part of the conduction band to generate the band gap, which generates the charge accumulations between the X and Ge atoms to form the

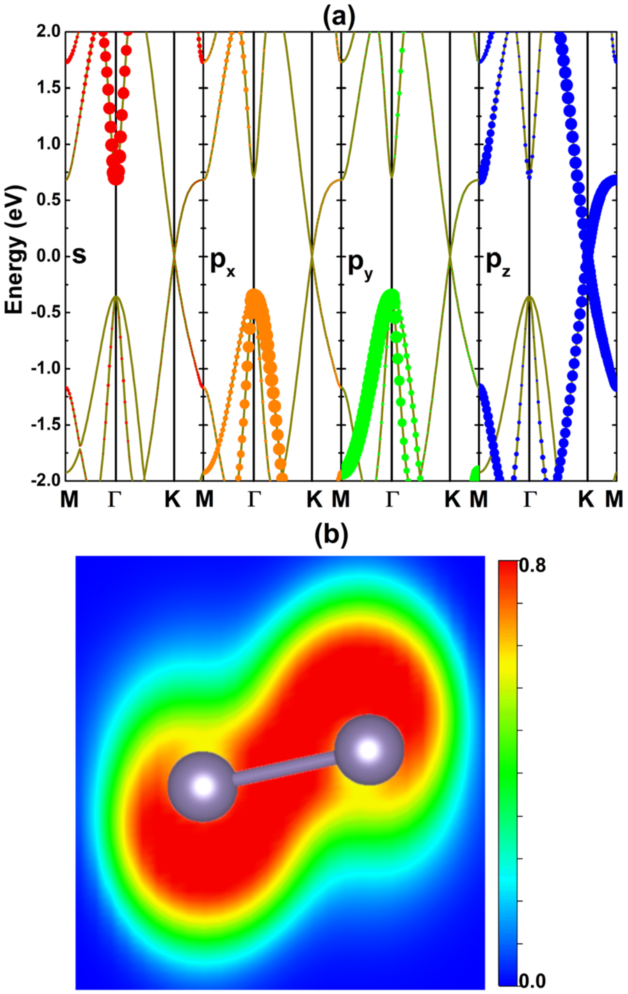

Fig. 2 (a) Orbital-decomposed band structure (the Fermi level is set to 0 eV) and (b) electron localization function of the germanene monolayer.

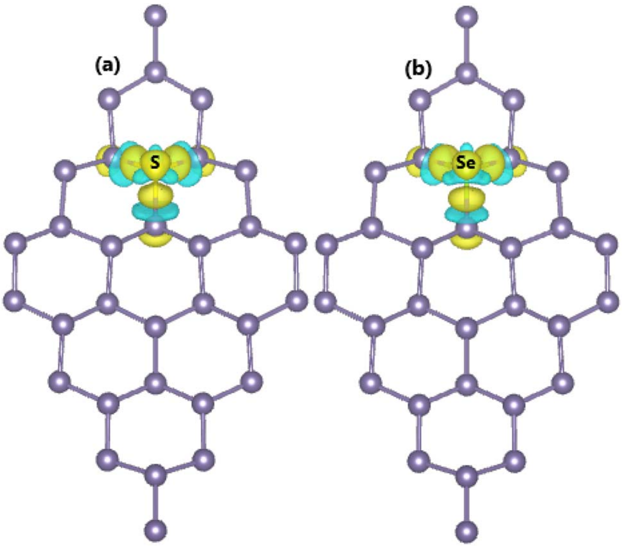

Fig. 3 Charge density difference in (a) 1S- and (b) 1Se-doped germanene monolayers (iso-surface value: 0.003 e Å$^{-3}$; yellow surface: charge enrichment; aqua surface: charge depletion).

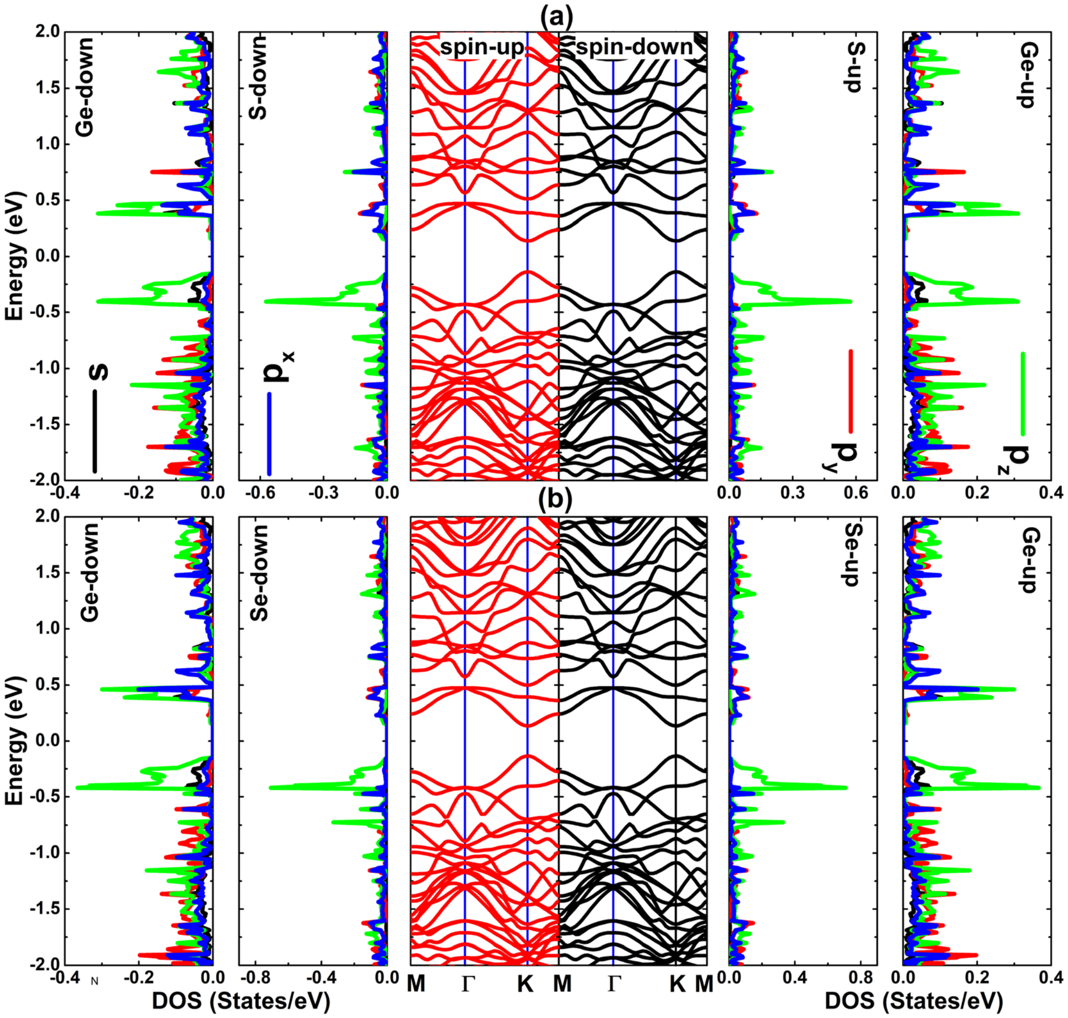

Fig. 4 Spin-resolved band structure, and projected density of states of the chalcogen impurity and its nearest neighboring Ge atom of (a) 1S- and (b) 1Se-doped germanene monolayers (the Fermi level is set to 0 eV).

covalent character as analyzed above. Specifically, the $p_z$ state of these atoms forms mainly the band structure around the Fermi level, where the $p_x$ and $p_y$ states also make contributions to the conduction band lower part.

The effects of doping level are also studied by increasing the number of impurities in the 4 × 4 × 1 germanene supercell. Specifically, two and four X impurities are considered. In these cases, the doped systems are denoted as 2X@mo and 4X@mo, respectively. It is found that no magnetism is induced regardless of the doping level, however the electronic band structures are affected considerably as observed in Fig. 5. Specifically, 2S and 2Se impurities keep the direct-gap semiconductor nature. Herein, energy gaps of 0.50 and 0.49 eV are obtained, respectively. Further increasing the chalcogen concentration, no significant change in the band gap is noted. Specifically, the 4S@mo and 4Se@mo systems have energy gaps of 0.45 and 0.46 eV, respectively. However, a direct-to-indirect gap transition is induced considering that the location of the conduction band minimum shifts to the region between the Γ and K points. In conclusion, our calculations suggest chalcogen doping as an efficient route to open the germanene monolayer band gap, where electronic properties can be controlled by the doping level.

### 3.3. Effects of doping with a single Mn atom

Herein, the impact of doping with Mn transition metal on the germanene monolayer's electronic and magnetic properties is studied. Firstly, single atom doping is considered, where 1Mn@mo is employed to denote the doped system. The charge density difference is calculated to analyze the interactions between the Mn impurity and the germanene monolayer, using the following expression: $\Delta\rho = \rho(1\text{Mn@mo}) - \rho(\text{mo}) - \rho(\text{Mn})$, where $\rho(1\text{Mn@mo})$, $\rho(\text{mo})$, and $\rho(\text{Mn})$ are the charge density of the 1Mn@mo system, germanene monolayer, and single Mn atom, respectively. From the visualization in Fig. 6a, it can be noted that the Mn impurity loses charge, while charge enrichment is found at its nearest neighboring Ge atom. This feature is derived from the less electronegative nature of the Mn atom in comparison to the Ge atom, such that Ge atoms attract the valence charge of the Mn atom. Our Bader charge analysis

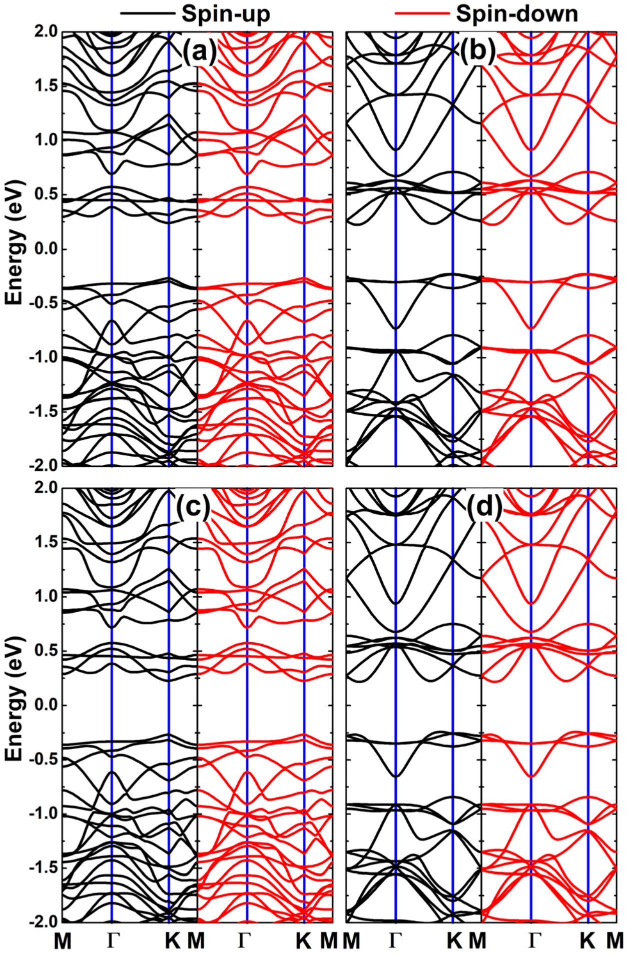

Fig. 5 Spin-resolved band structure of (a) 2S-, (b) 4S-, (c) 2Se-, and (d) 4Se-doped germanene monolayers (the Fermi level is set to 0 eV).

confirms that the Mn atom transfers a charge quantity of 0.46*e* to the host germanene monolayer.

It is found that Mn doping induces significant magnetization of the germanene monolayer, such that a total magnetic moment of $3.78\mu_B$ is obtained for the 1Mn@mo system. In this case, the Mn impurity has a local magnetic moment of $4.07\mu_B$ that is slightly larger than the overall value. The spin density displayed in Fig. 6b confirms that the Mn impurity produces primarily the magnetic moment of the 1Mn@mo system considering the large iso-surface concentrated at its site. Moreover, a little contribution from the Ge atoms closest to the doping site is also observed, exhibiting the antiparallel spin coupling with the Mn dopant atom that is the reason why the local magnetic moment of the Mn impurity is larger than the total value. In addition, we determine the magnetic anisotropy of the 1Mn@mo system – that is an important property to consider for practical application – using the criterion of magnetic anisotropy energy (MAE) calculated by:

$$\text{MAE} = E_x - E_z \quad (1)$$

where $E_x$ and $E_z$ refer to the system total energy that is calculated using a two-step approach: (1) self-consistent calculations without spin–orbit coupling (SOC), followed by (2) non-self-consistent calculations with SOC enabled setting the easy magnetization direction along the *x* ([100] direction) and *z* ([001] direction) axis, respectively. Our simulations provide a negative MAE value of −452.87 μeV, indicating that the in-plane magnetic anisotropy (IMA) is more stable than the perpendicular magnetic anisotropy (PMA). These results may suggest 1Mn-doped germanene as a prospective candidate for magnetic field sensing.

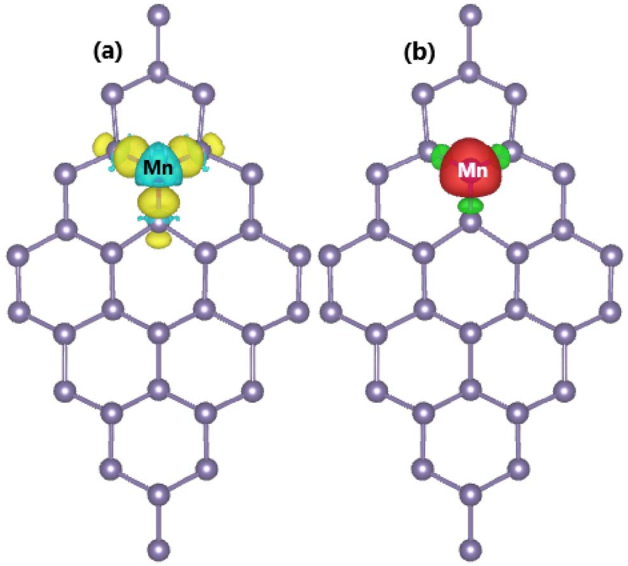

Fig. 6 (a) Charge density difference (iso-surface value: 0.003 e Å$^{-3}$; yellow surface: charge enrichment; aqua surface: charge depletion) and (b) spin density (iso-surface value: 0.005 e Å$^{-3}$) in the 1Mn-doped germanene monolayer.

The spin-polarized band structure and PDOS spectra of 1Mn@mo systems are given in Fig. 7. It can be noted that Mn doping induces spin polarization in the germanene monolayer, mostly around the Fermi level. Both spin states exhibit metallic character, asserting the germanene monolayer metallization induced by doping with a single Mn atom. PDOS spectra indicate that the metallic character of the spin-up state is produced mainly by the Mn-$d_{xz}$-$d_{x^2-y^2}$ states with little effect from the Ge-$p_{x,y,z}$ states. The Ge-$p_z$ state originates mainly the metallic character of the spin-down state. Therefore, it can be concluded that the electronic properties of the 1Mn@mo system are regulated mainly by the Mn impurity and its neighboring Ge atoms. From PDOS spectra, it is important to note significant electronic hybridization of Mn-d and Ge-p orbitals despite their difference in electronegativity, which is also a characteristic of 2D materials in which chemical bonds exhibit both covalent character (formed by the electronic hybridization) and ionic character (formed by the charge transfer).

### 3.4. Magnetic phase and effects of codoping with chalcogen atoms

In order to determine the stable magnetic phase in the Mn-doped germanene monolayer, we study the spin coupling of

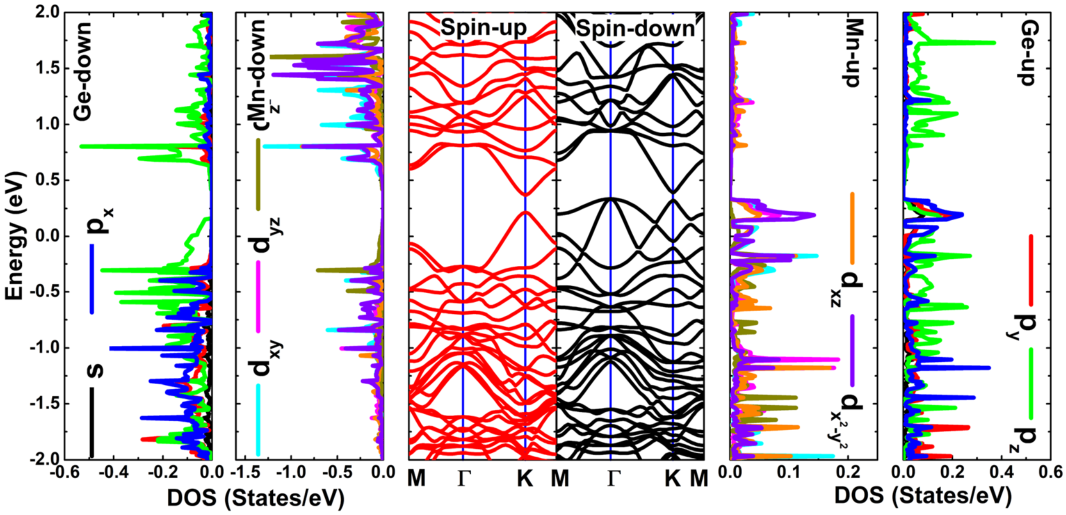

Fig. 7 Spin-resolved band structure, and projected density of states of the chalcogen impurity and its nearest neighboring Ge atom of the 1Mn-doped germanene monolayer (the Fermi level is set to 0 eV).

two Mn impurities in the 4× 4 × 1 supercell (named as the 2Mn@mo system). A ferromagnetic (FM) state simulated by Mn–Mn parallel spin coupling and antiferromagnetic (AFM) state modeled by Mn–Mn antiparallel spin coupling are considered. By calculating the total system energy, it is found that the AFM state has smaller energy than the FM state with a difference of 23.32 meV (see the illustration in Fig. 8a), confirming its stability in the 2Mn@mo system. Interestingly, further substitutional doping of an additional chalcogen atom (to form 2Mn+X@mo systems) induces the AFM-to-FM state transition as observed in Fig. 8b and c. Such that the FM state is stable in the 2Mn+S@mo and 2Mn+Se@mo systems, presenting energy differences of 47.42 and 48.99 meV as compared to the AFM state, respectively. From now on, we will only discuss the electronic and magnetic properties of the antiferromagnetic 2Mn@mo and ferromagnetic 2Mn+X@mo systems. For practical applications, the Curie temperature $T_C$ of ferromagnetic materials is essential, therefore we calculate this parameter using the mean-field approximation (MFA) as follows:

$$\frac{-3}{2}k_{B}T_{C} = \frac{\Delta E}{N} \tag{2}$$

where $k_B$, $\Delta E$, and $N$ denote the Boltzmann constant, energy difference between the FM and AFM states, and number of Mn atoms, respectively. According to our calculations, the 2Mn+S@mo and 2Mn+Se@mo systems have $T_C$ values of 183.52 and 189.59 K, respectively. However, the MFA generally overestimates the Curie temperature because of the inaccurate description of the magnetic percolation effects. Therefore, an empirical relation has been proposed to determine the lower limit of this parameter as follows: $T_C^{\text{empirical}} = 0.51 \times T_C^{\text{MFA}}$.[40] From this relation, lower $T_C$ limits for the 2Mn+S@mo and 2Mn+Se@mo systems are calculated to be 93.60 and 96.69 K, respectively.

In the AFM state, a zero overall magnetic moment is obtained for the 2Mn@mo system, in which each Mn impurity has a local value of 4.07$\mu_B$ (with opposite signs). While, the ferromagnetic 2Mn+S@mo and 2Mn+Se@mo systems have large total magnetic moments of 8.08 and 8.14$\mu_B$, respectively. In these cases, Mn dopant atoms have local values between 4.08 and 4.17$\mu_B$, producing mainly the system magnetic moment. Meanwhile, S and Se atoms have quite small values of $-0.05\mu_B$, suggesting their negligible contribution to the system magnetism. Using eqn (1), a positive MAE value of 187.08 μeV is obtained for the 2Mn@mo system, indicating its PMA. Meanwhile, IMA is found in the cases of the 2Mn+S@mo and 2Mn+Se@mo systems with negative MAE values of −65.27 and −261.14 μeV, respectively. This interesting switching can be attributed to the interactions between the Mn-3d orbital with its neighboring environment. Specifically, the Mn-3d orbital interacts with the out-of-plane $p_z$ state of the nearest neighboring Te atoms to generate the PMA in the 2Mn@mo system. In the cases of codoping, Mn atoms transfer more charge to the S/Se atoms because of their more electronegative nature compared to the Te atom, therefore the S/Se-p orbital is more occupied than the Te-p orbital. Consequently, the interactions between the Mn-3d orbital and the in-plane S/Se-$p_{x,y}$ states become strong, inducing the in-plane magnetic anisotropy.

The spin-polarized band structures of 2Mn-, 2Mn+S-, and 2Mn+Se-doped germanene monolayers are displayed in Fig. 9. From panel a, one can see the spin-symmetric profile of the antiferromagnetic 2Mn@mo system, where both spin states exhibit semiconductor character with a small K–K direct gap of 0.05 eV, which increases slightly to 0.06 eV when the spin–orbit coupling is included. These results suggest the antiferromagnetic semiconductor nature in germanene induced by 2Mn doping. The presence of chalcogen impurities will metallize the spin-up state and open the spin-down state band gap as observed in panels b–c, giving place to the formation of the half-metallic nature. Specifically, the semiconductor spin-down state of the 2Mn+S@mo and 2Mn+Se@mo systems has an energy gap of 0.24 and 0.26 eV, respectively. These results demonstrate the

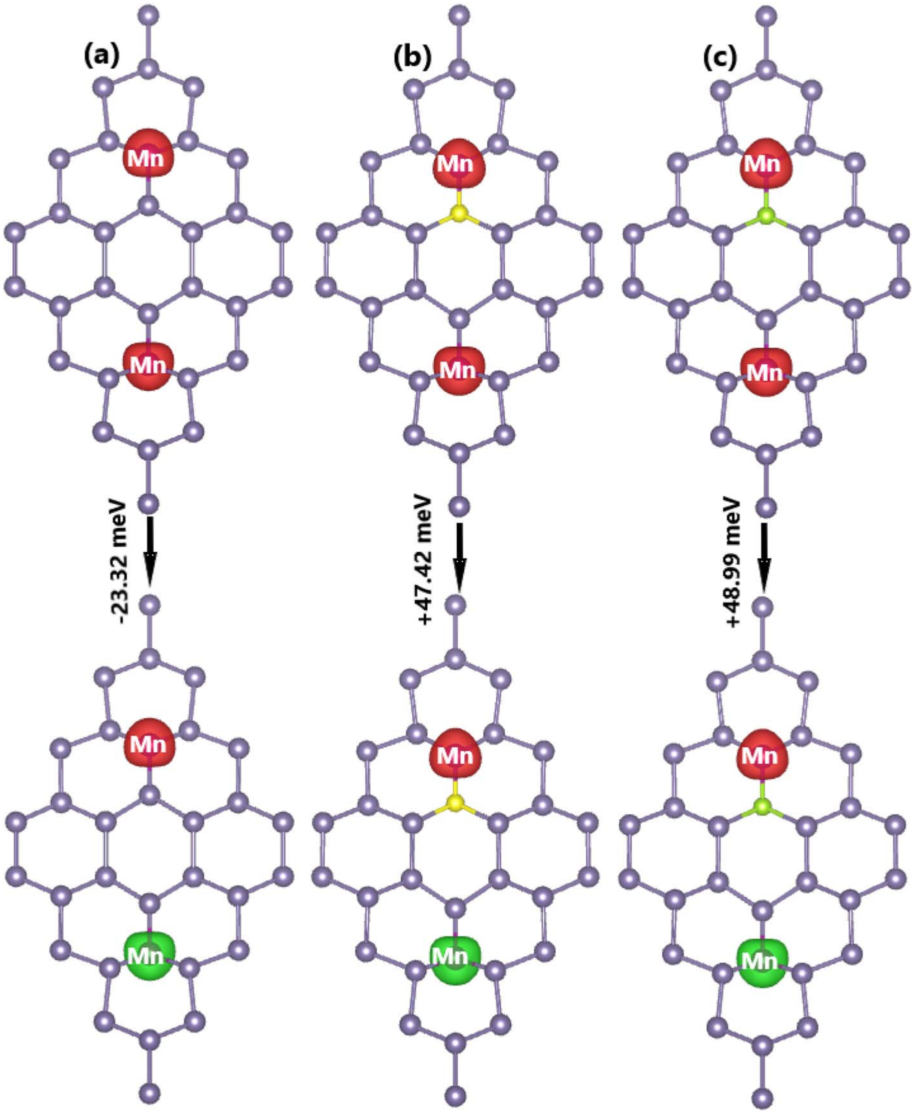

Fig. 8 Spin density (iso-surface value: 0.01 e Å$^{-3}$; red surface: positive spin density; green surface: negative spin density) and energy difference between FM and AFM states of (a) 2Mn-, (b) 2Mn+S-, and (c) 2Mn+Se-doped germanene monolayers.

effectiveness of codoping with Mn and chalcogen atoms to develop the half-metallic ferromagnetism with in-plane magnetic anisotropy in the semimetal germanene monolayer, which is obtained by the band gap opening induced by chalcogen doping combined with the magnetism engineering induced by Mn doping. Such that, the codoped 2Mn+X@mo systems can be recommended as promising 2D candidates for magnetic field sensing. All the magnetic and electronic properties results for the doped germanene systems are summarized in Table 1.

### 3.5. Stability of the doped/codoped systems

To determine the energy that should be supplied to realize the doping processes in the germanene monolayer, we calculate the formation energy $E_f$ using the following expression:

$$E_f = \frac{E(\text{do@mo}) - E(\text{mo}) + n_{\text{Ge}}\mu_{\text{Ge}} - n_X\mu_X - n_{\text{Mn}}\mu_{\text{Mn}}}{n_{\text{Ge}}} \quad (3)$$

$E$(do@mo) and $E$(mo) are total energy of the doped and bare germanene monolayer, respectively; $n_{\text{Ge}}$ and $n_{\text{X/Mn}}$ denote the number of removed Ge atoms and incorporated X/Mn atoms ($n_{\text{Ge}} = n_X + n_{\text{Mn}}$), respectively; $\mu_{\text{Ge}}$ and $\mu_{\text{X/Mn}}$ refer to the chemical potential of Ge and X/Mn atoms, respectively, which are calculated from their most stable bulk phase. Results are plotted in Fig. 10a. Note that chalcogen doping processes are exothermic as suggested by the negative $E_f$ values between −0.47 and −0.17 eV per atom. Meanwhile, doping with Mn impurities requires supplying additional energy of 1.85 (single impurities) and 1.78 eV per atom (two impurities). Codoping with chalcogen atoms may reduce considerably the required energies to 0.65/0.67 eV per atom. Experimentally, doping processes are often realized using ion/atom irradiation or bombardment, therefore our obtained results of formation energy may provide useful information to design the doping processes. Once formed, structural–chemical stability of the

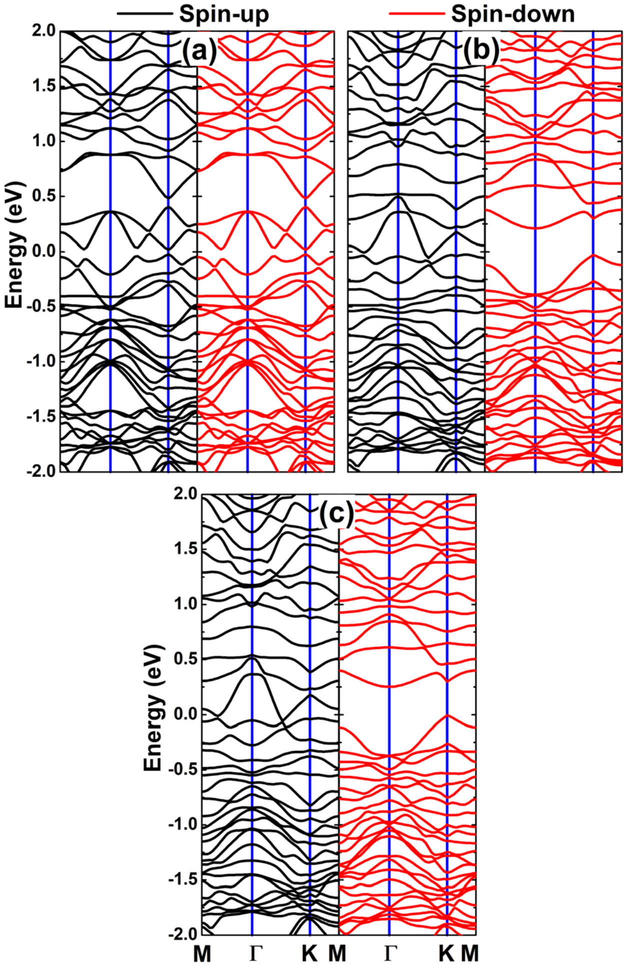

Fig. 9 Spin-resolved band structures of (a) 2Mn-, (b) 2Mn+S-, and (c) 2Mn+Se-doped germanene monolayers (the Fermi level is set to 0 eV).

doped germanene systems is examined by means of cohesive energy $E_c$ computed as follows:

$$E_c = \frac{E(\text{do@mo}) - m_{\text{Ge}}E_{\text{Ge}} - m_{\text{X}}E_{\text{X}} - m_{\text{Mn}}E_{\text{Mn}}}{m_{\text{Ge}} + m_{\text{X}} + m_{\text{Mn}}} \tag{4}$$

herein, $m_i$ and $E_i$ denote the number of atom "*i*" in the system and energy of an isolated atom "*i*", respectively. From Fig. 10b, it can be noted that all the doped germanene systems have negative $E_c$ values between −3.29 and −3.07 eV per atom. The negative $E_c$ values indicate that the doped/codoped germanene systems are structurally–chemically stable.

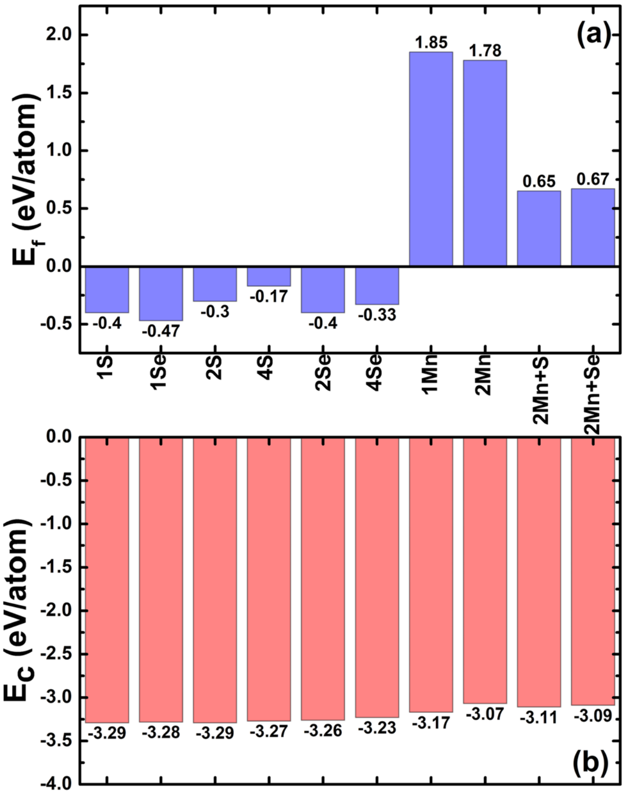

Fig. 10 (a) Formation energy and (b) cohesive energy of the doped germanene monolayers.

In addition, we also carried out *ab initio* molecular dynamics (AIMD) simulations at 300 K to check the thermal stability using canonical ensemble and Nosé–Hoover thermostat.[41,42] The simulations are recorded for 5 ps with time steps of 2 fs (2500 steps). Fig. 11 visualizes the final atomic structures after AIMD simulations. Distortion of hexagonal rings, mostly around the doping sites, can be noted. Overall, the hexagonal structural configuration is well preserved without any reconstruction nor broken bonds. These results confirm good thermal stability of the studied doped/codoped germanene monolayers.

Table 1 Total magnetic moment $M_t$ ($\mu_B$), energy difference between FM and AFM states $\Delta E$ (meV), magnetic anisotropy energy MAE (μeV), energy gap $E_g$ (eV; spin-up/spin-down; M = metallic), and gap path along the high-symmetry direction of the doped germanene systems (N/A: not applicable)

| | $M_t$ | $\Delta E$ | MAE | $E_g$ | Gap path |
|---|---|---|---|---|---|
| 1S@mo | 0.00 | N/A | N/A | 0.28/0.28 | K–K |
| 1Se@mo | 0.00 | N/A | N/A | 0.27/0.27 | K–K |
| 2S@mo | 0.00 | N/A | N/A | 0.50/0.50 | K–K |
| 4S@mo | 0.00 | N/A | N/A | 0.45/0.45 | K–MΓ |
| 2Se@mo | 0.00 | N/A | N/A | 0.49/0.49 | K–K |
| 4Se@mo | 0.00 | N/A | N/A | 0.46 | ΓK–MΓ |
| 1Mn@mo | 3.78 | N/A | −452.87 (IMA) | M/M | N/A |
| 2Mn@mo | 0.00 | −23.32 (AFM) | +187.08 (PMA) | 0.05/0.05 | K–K |
| 2Mn+S@mo | 8.08 | +47.42 (FM) | −65.27 (IMA) | M/0.24 | K–Γ |
| 2Mn+Se@mo | 8.14 | +48.99 (FM) | −261.14 (IMA) | M/0.26 | K–Γ |

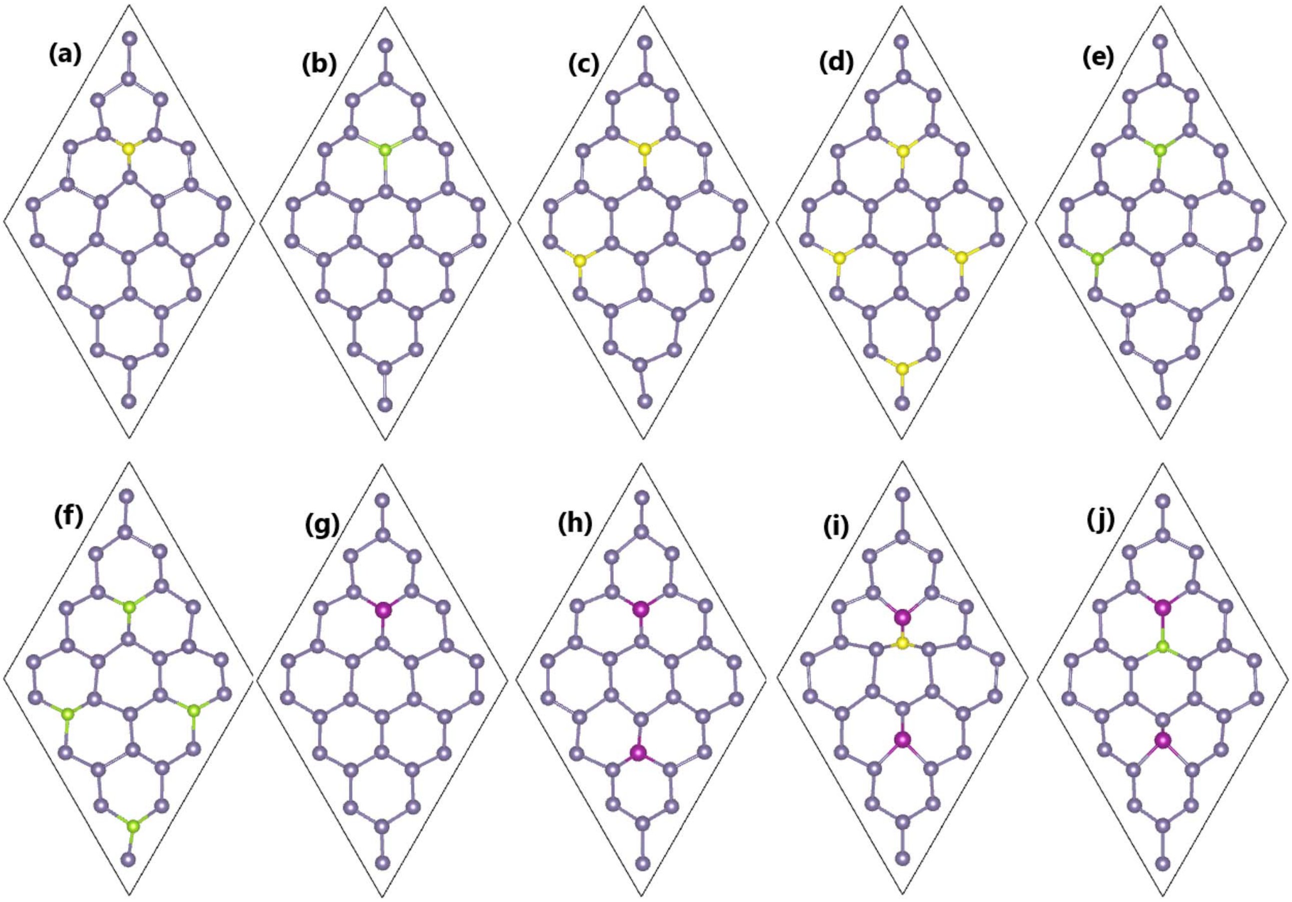

Fig. 11 Final atomic structures after AIMD simulations of (a) 1S-, (b) 1Se-, (c) 2S-, (d) 4S-, (e) 2Se-, (f) 4Se-, (g) 1Mn-, (h) 2Mn-, (i) Mn+S-, and (j) Mn+Se-doped germanene monolayers.

## 4. Conclusions

In summary, first-principles calculations have been performed to investigate the effects of doping/codoping with chalcogen (X = S and Se) atoms and Mn transition metal on the germanene monolayer's electronic and magnetic properties. The band structure of the pristine monolayer is formed mainly by Ge-s-$p_{x,y,z}$ states, where the semimetal character is originated mainly from the $p_z$ state. It is found that the covalent character of the Ge–Ge chemical bond is generated by the electronic hybridization, similar to other 2D monoelemental monolayers. The effective band gap opening of the germanene monolayer can be achieved by doping with S and Se atoms, which can be attributed to the charge transfer from the outermost Ge-4p orbital to S-3p/Se-4p orbitals, such that the upper part of the valence band is produced mainly by the S(Se)-$p_z$ state, while the Ge-$p_z$ state originates mainly the lower part of the conduction band. The band gap increases with increasing the impurity concentration. The germanene monolayer is significantly magnetized by doping with Mn transition metal that acts as a charge loser agent in the doped system. A magnetic moment is produced primarily by the Mn impurity, where a little contribution from nearest neighboring Ge atoms is also confirmed that exhibit antiparallel spin coupling with the Mn impurity. The AFM state with PMA is stable in the Mn-doped system, exhibiting a smaller energy than the FM state with an energy difference of 23.32 meV. In this case, the band gap is slightly opened to 0.05 eV. Interestingly, the AFM-to-FM state transition is achieved by codoping with S and Se atoms, where the energy differences are 47.42 and 48.99 meV, respectively. Additional chalcogen impurities metallize the spin-up state, while large band gaps are obtained for the spin-down state, confirming the successful development of half-metallic ferromagnetism in the germanene monolayer. Moreover, the PMA-to-IMA switching produced by codoping effects also suggests effective control of the magnetic anisotropy. Our results may pave solid ways to develop half-metallic ferromagnetism in the semimetal germanene monolayer towards spintronic applications, which could be applied for other 2D semimetal materials.

## Conflicts of interest

The authors declare that they have no known competing financial interests or personal relationships that could have appeared to influence the work reported in this paper.

## Data availability

Data will be provided upon request to the authors.

Supplementary information: the convergence testing of the employed computational parameters. See DOI: https://doi.org/10.1039/d5ra06032j.

## Acknowledgements

Calculations were performed in DGCTIC-UNAM Supercomputing Center (projects LANCAD-UNAM-DGTIC-368 and LANCAD-UNAM-DGTIC-422).

## References

1 P. R. Wallace, The band theory of graphite, *Phys. Rev.*, 1947, **71**(9), 622.

2 K. S. Novoselov, A. K. Geim, S. V. Morozov, D.-e. Jiang, Y. Zhang, S. V. Dubonos, I. V. Grigorieva and A. A. Firsov, Electric field effect in atomically thin carbon films, *Science*, 2004, **306**(5696), 666–669.

3 D. Abergel, V. Apalkov, J. Berashevich, K. Ziegler and T. Chakraborty, Properties of graphene: a theoretical perspective, *Adv. Phys.*, 2010, **59**(4), 261–482.

4 M. J. Allen, V. C. Tung and R. B. Kaner, Honeycomb carbon: a review of graphene, *Chem. Rev.*, 2010, **110**(1), 132–145.

5 K. Takeda and K. Shiraishi, Theoretical possibility of stage corrugation in Si and Ge analogs of graphite, *Phys. Rev. B: Condens. Matter Mater. Phys.*, 1994, **50**(20), 14916.

6 S. Cahangirov, M. Topsakal, E. Aktürk, H. Şahin and S. Ciraci, Two-and one-dimensional honeycomb structures of silicon and germanium, *Phys. Rev. Lett.*, 2009, **102**(23), 236804.

7 L. Li, S.-z. Lu, J. Pan, Z. Qin, Y.-q. Wang, Y. Wang, G.-y. Cao, S. Du and H.-J. Gao, Buckled germanene formation on Pt(111), *Adv. Mater.*, 2014, **26**(28), 4820–4824.

8 L. Kesper, J. A. Hochhaus, M. Schmitz, M. G. Schulte, U. Berges and C. Westphal, Tracing the structural evolution of quasi-freestanding germanene on Ag (111), *Sci. Rep.*, 2022, **12**(1), 7559.

9 M. Ge, M. Zong, D. Xu, Z. Chen, J. Yang, H. Yao, C. Wei, Y. Chen, H. Lin and J. Shi, Freestanding germanene nanosheets for rapid degradation and photothermal conversion, *Mater. Today Nano*, 2021, **15**, 100119.

10 J. Yuhara, H. Shimazu, K. Ito, A. Ohta, M. Araidai, M. Kurosawa, M. Nakatake and G. Le Lay, Germanene epitaxial growth by segregation through Ag(111) thin films on Ge(111), *ACS Nano*, 2018, **12**(11), 11632–11637.

11 S. Suzuki, T. Iwasaki, K. K. H. De Silva, S. Suehara, K. Watanabe, T. Taniguchi, S. Moriyama, M. Yoshimura, T. Aizawa and T. Nakayama, Direct growth of germanene at interfaces between van der Waals materials and Ag(111), *Adv. Funct. Mater.*, 2021, **31**(5), 2007038.

12 J. Fang, P. Zhao and G. Chen, Germanene growth on Al(111): A case study of interface effect, *J. Phys. Chem. C*, 2018, **122**(32), 18669–18681.

13 C.-H. Lin, A. Huang, W. W. Pai, W.-C. Chen, T.-Y. Chen, T.-R. Chang, R. Yukawa, C.-M. Cheng, C.-Y. Mou, I. Matsuda, *et al.*, Single-layer dual germanene phases on Ag(111), *Phys. Rev. Mater.*, 2018, **2**(2), 024003.

14 N. Liu, G. Bo, Y. Liu, X. Xu, Y. Du and S. X. Dou, Recent progress on germanene and functionalized germanene: preparation, characterizations, applications, and challenges, *Small*, 2019, **15**(32), 1805147.

15 A. Acun, L. Zhang, P. Bampoulis, M. v. Farmanbar, A. van Houselt, A. Rudenko, M. Lingenfelder, G. Brocks, B. Poelsema, M. Katsnelson, *et al.*, Germanene: the germanium analogue of graphene, *J. Phys.: Condens. Matter*, 2015, **27**(44), 443002.

16 Z. Ni, Q. Liu, K. Tang, J. Zheng, J. Zhou, R. Qin, Z. Gao, D. Yu and J. Lu, Tunable bandgap in silicene and germanene, *Nano Lett.*, 2012, **12**(1), 113–118.

17 M. Ye, R. Quhe, J. Zheng, Z. Ni, Y. Wang, Y. Yuan, G. Tse, J. Shi, Z. Gao and J. Lu, Tunable band gap in germanene by surface adsorption, *Phys. E Low-dimens. Syst. Nanostruct.*, 2014, **59**, 60–65.

18 D. Hoat, D. K. Nguyen, R. Ponce-Perez, J. Guerrero-Sanchez, V. Van On, J. Rivas-Silva and G. H. Cocoletzi, Opening the germanene monolayer band gap using halogen atoms: An efficient approach studied by first-principles calculations, *Appl. Surf. Sci.*, 2021, **551**, 149318.

19 M. Houssa, E. Scalise, K. Sankaran, G. Pourtois, V. Afanas'ev and A. Stesmans, Electronic properties of hydrogenated silicene and germanene, *Appl. Phys. Lett.*, 2011, **98**(22), 223107.

20 Q. Yao, L. Zhang, N. Kabanov, A. Rudenko, T. Arjmand, H. Rahimpour Soleimani, A. Klavsyuk and H. Zandvliet, Bandgap opening in hydrogenated germanene, *Appl. Phys. Lett.*, 2018, **112**(17), 171607.

21 A. Hirohata and K. Takanashi, Future perspectives for spintronic devices, *J. Phys. D: Appl. Phys.*, 2014, **47**(19), 193001.

22 I. Žutić, J. Fabian and S. D. Sarma, Spintronics: Fundamentals and applications, *Rev. Mod. Phys.*, 2004, **76**(2), 323.

23 E. C. Ahn, 2D materials for spintronic devices, *npj 2D Mater. Appl.*, 2020, **4**(1), 17.

24 Y. P. Feng, L. Shen, M. Yang, A. Wang, M. Zeng, Q. Wu, S. Chintalapati and C.-R. Chang, Prospects of spintronics based on 2D materials, *Wiley Interdiscip. Rev.: Comput. Mol. Sci.*, 2017, **7**(5), e1313.

25 Y. Liu, C. Zeng, J. Zhong, J. Ding, Z. M. Wang and Z. Liu, Spintronics in two-dimensional materials, *Nano-Micro Lett.*, 2020, **12**(1), 93.

26 J. Xu, W. Li and Y. Hou, Two-dimensional magnetic nanostructures, *Trends Chem.*, 2020, **2**(2), 163–173.

27 M. Hossain, B. Qin, B. Li and X. Duan, Synthesis, characterization, properties and applications of two-dimensional magnetic materials, *Nano Today*, 2022, **42**, 101338.

28 P. Huang, P. Zhang, S. Xu, H. Wang, X. Zhang and H. Zhang, Recent advances in two-dimensional ferromagnetism: materials synthesis, physical properties and device applications, *Nanoscale*, 2020, **12**(4), 2309–2327.

29 P. Aghdasi, S. Yousefi and R. Ansari, Doping-induced changes in the structural and mechanical properties of

germanene monolayers: A DFT-based study, *Mater. Sci. Semicond. Process.*, 2024, **174**, 108246.

30 W. Kohn and L. J. Sham, Self-consistent equations including exchange and correlation effects, *Phys. Rev.*, 1965, **140**(4A), A1133.

31 G. Kresse and J. Furthmüller, Efficiency of ab-initio total energy calculations for metals and semiconductors using a plane-wave basis set, *Comput. Mater. Sci.*, 1996, **6**(1), 15–50.

32 G. Kresse and J. Furthmüller, Efficient iterative schemes for ab initio total-energy calculations using a plane-wave basis set, *Phys. Rev. B: Condens. Matter Mater. Phys.*, 1996, **54**(16), 11169.

33 J. P. Perdew, K. Burke and M. Ernzerhof, Generalizedgradient approximation made simple, *Phys. Rev. Lett.*, 1996, **77**(18), 3865.

34 S. L. Dudarev, G. A. Botton, S. Y. Savrasov, C. Humphreys and A. P. Sutton, Electron-energy-loss spectra and the structural stability of nickel oxide: An LSDA+U study, *Phys. Rev. B: Condens. Matter Mater. Phys.*, 1998, **57**(3), 1505.

35 Y. Wang, S. Li and J. Yi, Transition metal-doped tin monoxide monolayer: a first-principles study, *J. Phys. Chem. C*, 2018, **122**(8), 4651–4661.

36 T. V. Vu, V. H. Chu, J. Guerrero-Sanchez and D. Hoat, Regulating the electronic and magnetic properties of a SnSSe Janus monolayer toward optoelectronic and spintronic applications, *ACS Appl. Electron. Mater.*, 2024, **6**(5), 3647–3656.

37 H. J. Monkhorst and J. D. Pack, Special points for Brillouin-zone integrations, *Phys. Rev. B*, 1976, **13**(12), 5188.

38 H. Şahin, S. Cahangirov, M. Topsakal, E. Bekaroglu, E. Akturk, R. T. Senger and S. Ciraci, Monolayer honeycomb structures of group-IV elements and III-V binary compounds: First-principles calculations, *Phys. Rev. B: Condens. Matter Mater. Phys.*, 2009, **80**(15), 155453.

39 S. Balendhran, S. Walia, H. Nili, S. Sriram and M. Bhaskaran, Elemental analogues of graphene: silicene, germanene, stanene, and phosphorene, *Small*, 2015, **11**(6), 640–652.

40 Z. Liu, J. Liu and J. Zhao, $YN_2$ monolayer: Novel p-state Dirac half metal for high-speed spintronics, *Nano Res.*, 2017, **10**(6), 1972–1979.

41 S. Nosé, A unified formulation of the constant temperature molecular dynamics methods, *J. Chem. Phys.*, 1984, **81**(1), 511–519.

42 W. G. Hoover, Canonical dynamics: Equilibrium phase-space distributions, *Phys. Rev. A*, 1985, **31**(3), 1695.